Supporting Information for

Modular Artificial Cupredoxins

Samuel I. Mann,[§] Tillmann Heinisch,[¶] Andrew C. Weitz,[†] Michael P. Hendrich,[†]* Thomas R. Ward,[¶]* A. S. Borovik[§]*

Department of Chemistry, University of California-Irvine, 1102 Natural Sciences II, Irvine, CA 92697

Department of Chemistry, University of Basel, Spitalstrasse 51, CH-4056 Basel, Switzerland

Department of Chemistry, Carnegie Mellon University, Pittsburgh, PA 15213

Contents

General Methods. All commercially available reagents were obtained of the highest purity and used as received. Dimethylsulfoxide, *N*,*N*-dimethylformamide, and diethylether were degassed with argon and dried by vacuum filtration through activated alumina according to the procedure by Grubbs.[1] Triethylamine and ethylenediamine were distilled from KOH.

Thin-layer chromatography (TLC) was performed on Whatman 250 μm layer 6 Å glass-backed silica gel plates. Eluted plates were visualized using UV light. Silica gel chromatography was performed with the indicated solvent system using Fisher reagent silica gel 60 (230-400 mesh). Biotin pentafluorophenol ester,[2] di[2-(2-pyridyl)ethyl]hydroxylamine,[3] and di[2-(2-pyridyl)ethyl]amine[3] were prepared according to literature procedures.

Preparative Methods

Scheme S1. Synthetic Route for the Preparation of the biot-R-dpea Ligands.

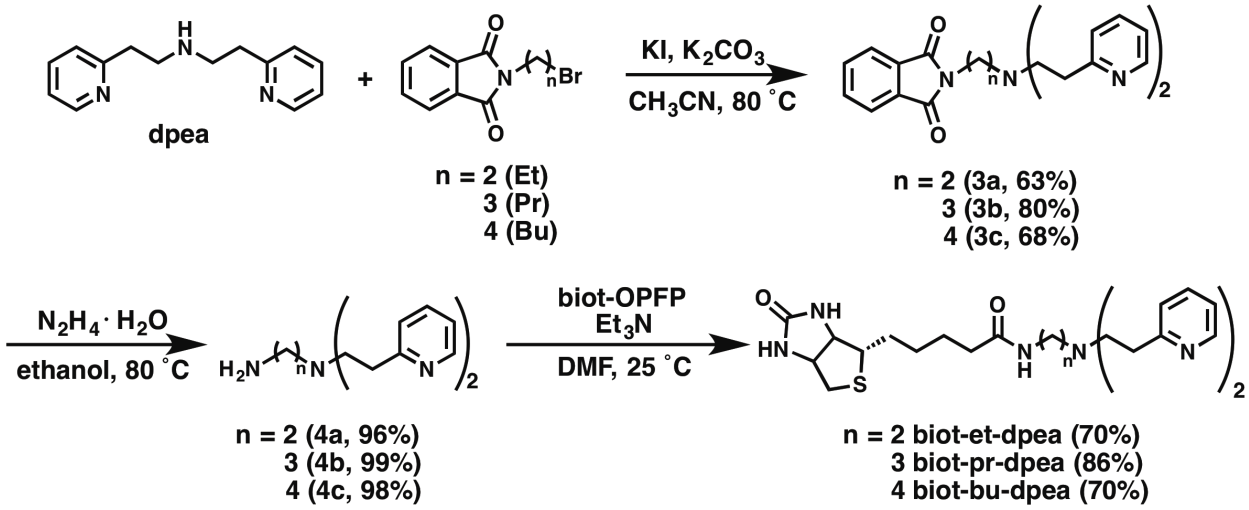

2-(2-(bis(2-(pyridin-2-yl)ethyl)amino)ethyl)isoindoline-1,3-dione (3a).[4]. Di[2-(2-pyridyl)ethyl]amine (1.01 g, 4.44 mmol), bromoethylphthalimide (1.24 g, 4.88 mmol), KI (0.147 g, 0.890 mmol), and K_2CO_3 (2.45 g, 17.7 mmol) were mixed in 40 mL acetonitrile and refluxed for 24 hours. The solution was cooled to room temperature, filtered and the solvent was removed under vacuum. The red-brown residue was dissolved in dichloromethane and washed with 3 x 25 mL aqueous $NaHCO_3$ and 1 x 25 mL H_2O. The red-brown oil was dissolved in 15 mL conc. HCl and washed with 2 x 20 mL dichloromethane. The aqueous layer was carefully neutralized with solid $NaHCO_3$ and extracted in 3 x 20 mL

dichloromethane. The solvent was dried over $MgSO_4$ and removed under vacuum to yield crude **3a**. The crude product was purified via column chromatography with silica gel (methanol:acetone (1:4)) to yield pure **3a** as a yellow oil (1.11 g, 63%). ^{1}H NMR (600 MHz, DMSO-d_6) δ 8.45 (d, J = 4.2 Hz, 2H), 7.82 (q, J = 3.7 Hz, 2H), 7.71 (q, J = 3.6 Hz, 2H), 7.45 (td, J = 9.2, 1.9 Hz, 2H), 7.08 (d, J = 8.5 Hz, 2H), 7.02 (t, J = 7.0 Hz, 2H), 3.75 (t, J = 8.0 Hz, 1H), 2.98 (t, J = 9.8 Hz, 4H), 2.86 (t, J = 9.7 Hz, 6H); ^{13}C NMR (125 MHz, DMSO-d_6) δ 168.3, 160.5, 149.2, 136.1, 133.8, 132.3, 123.4, 123.2, 121.0, 77.4, 77.1, 53.9, 53.5, 51.2, 36.2, 36.1; MS (ES, MeOH) *m / z* calcd for $C_{24}H_{24}N_4O_2$ $[M + H]^+$ 401.2, found 401.1; ATR-IR (neat, cm^{-1}, selected bands): 3060, 3005, 2947, 2810, 1771, 1701, 1590, 1568, 1473, 1434, 1395, 1355, 1322, 1184, 1102, 1085, 992, 749, 718, 625.

2-(3-(bis(2-(pyridin-2-yl)ethyl)amino)propyl)isoindoline-1,3-dione (3b) was prepared following the same procedure as described above for **3a** and isolated analogously as a yellow oil in 80% yield (1.22 g). ^{1}H NMR (500 MHz, DMSO-d_6) δ 8.49 (d, J = 5.1 Hz, 2H), 7.84 (q, J = 3.6 Hz, 2H), 7.71 (q, J = 3.7 Hz, 2H), 7.56 (td, J = 9.2, 1.6 Hz, 2H), 7.15 (d, J = 9.2 Hz, 2H), 7.09 (t, J = 6.8 Hz, 2H), 3.66 (t, J = 8.6 Hz, 2H), 2.99 (br s, 8H), 2.71 (br s, 2H), 1.89 (br s, 2H); ^{13}C NMR (125 MHz, DMSO-d_6) δ 168.4, 149.3, 136.4, 134.0, 133.9, 132.2, 123.6, 123.3, 121.3, 53.7, 51.6, 36.3, 35.6, 26.3; HRMS (ES, MeOH) *m / z* calcd for $C_{25}H_{26}N_4O_2$ $[M + H]^+$ 415.2134, found 415.2132; ATR-IR (neat, cm^{-1}, selected bands): 2941, 2810, 1769, 1705, 1589, 1568, 1473, 1434, 1394, 1365, 1188, 1148, 1122, 1088, 1038, 992, 889, 746, 719, 603.

2-(4-(bis(2-(pyridin-2-yl)ethyl)amino)butyl)isoindoline-1,3-dione (3c) was prepared with the analogous procedure as **3a** to yield **3c** as a yellow oil (0.99 g, 68%). ^{1}H NMR (600 MHz, DMSO-d_6) δ 8.48 (d, J = 3.6 Hz, 2H), 7.84 (q, J = 3.0 Hz, 2H), 7.71 (q, J = 3.0 Hz, 2H), 7.56 (t, J = 7.8 Hz, 2H), 7.13 (br, 2H), 7.09 (t, J = 5.4 Hz, 2H), 3.65 (t, J = 6.6 Hz, 2H), 2.97 (br s, 8H), 2.63 (br s, 2H), 1.61 (br s, 3H), 1.51 (br s, 2H); ^{13}C NMR (125 MHz, DMSO-d_6) δ 168.5,

160.1, 149.2, 136.4, 134.0, 132.2, 123.6, 123.3, 121.3, 53.8, 53.3, 37.8, 35.3, 26.4, 24.1; MS (ES, MeOH) *m / z* calcd for $C_{26}H_{28}N_4O_2$ $[M + H]^+$ 429.23, found 429.19.

N,N-bis(2-(pyridin-2-yl)ethyl)ethane-1,2-diamine (4a).[4] Hydrazine monohydrate (0.795 mL, 16.3 mmol) and **3a** (1.40 g, 3.27 mmol) were dissolved in 30 mL of absolute ethanol and the solution was refluxed for 3 hours. The phthalhydrazide precipitated as a white solid and was removed via filtration. The ethanol was removed under vacuum and the residue was dissolved in $CHCl_3$ and washed with 2 x 10 mL 1 M NaOH to remove any remaining phthalhydrazide. The organic layer was dried over $MgSO_4$, volatiles were removed under reduced pressure, and the product was isolated as a brown oil (0.957 g, 98%). ^{1}H NMR (500 MHz, $CDCl_3$) δ 8.53 (d, J = 4.2 Hz, 2H), 7.54 (td, J = 7.8, 1.6 Hz, 2H), 7.10 (app. t, J= 5.3 Hz, 2H), 7.05 (app. d, J = 7.8 Hz, 2H), 2.92 (m, 8H), 2.64 (t, J = 5.0 Hz, 2H), 2.58 (t, J = 5.0 Hz, 2H); ^{13}C NMR (125 MHz, $CDCl_3$) δ 160.9, 149.4, 136.2, 123.6, 121.2, 56.8, 54.2, 39.8, 36.3; HRMS (ES, MeOH) *m / z* calcd for $C_{16}H_{22}N_4$ $[M + H]^+$ 271.1923, found 271.1445; ATR-IR (neat ,cm^{-1}, selected bands): 3358, 3273, 2957, 2821, 1596, 1568, 1476, 1435, 1360, 1306, 1149, 1114, 1079, 1074, 999, 758, 632.

N,N-bis(2-(pyridin-2-yl)ethyl)propane-1,3-diamine (4b) was prepared analogously to the above procedure for **4a** to yield **4b** as a yellow oil (0.989 g, 99%). ^{1}H NMR (600 MHz, $CDCl_3$) δ 8.52 (d, J = 4.2 Hz, 2H), 7.56 (td, J = 7.8, 1.2 Hz, 2H), 7.10 (m, 4H), 2.92 (s, 8H), 2.61 (q, J = 6.6 Hz, 4H), 1.56 (quin, J = 7.2 Hz, 2H); ^{13}C NMR (125 MHz, $CDCl_3$) δ 160.7, 149.3, 136.3, 123.5, 121.2, 54.1, 51.8, 40.4, 35.9, 30.1; HRMS (ES, MeOH) *m / z* calcd for $C_{17}H_{24}N_4$ $[M + H]^+$ 285.2001, found 285.1690; ATR-IR (neat, cm-1, selected bands): 3356, 2935, 2812, 1642, 1591, 1568, 1475, 1434, 1355, 1309, 1150, 1120, 1089, 1052, 993, 751, 631, 606.

N,N-bis(2-(pyridin-2-yl)ethyl)butane-1,4-diamine (4c) was prepared following an analogous procedure for **4a** to afford **4c** as a yellow oil in (0.935 g,98% yield). ^{1}H NMR (500 MHz, $CDCl_3$) δ 8.52 (d, J = 4.1 Hz, 2H), 7.56 (t, J = 8.6 Hz, 2H), 7.11 (t, J = 7.8 Hz, 4H), 2.93 (s,

8H), 2.65 (t, J = 6.8 Hz, 2H), 2.56 (t, J = 7.3 Hz, 2H), 2.36 (br, 2H), 1.46 (quin, J = 6.8 Hz, 2H), 1.37 (quin, J = 6.9 Hz, 2H); ^{13}C NMR (125 MHz, $CDCl_3$) δ 160.8, 149.3, 136.3, 1123.5, 121.2, 54.1, 53.9, 42.1, 36.1, 31.5, 24.8; HRMS (ES, MeOH) *m / z* calcd for $C_{18}H_{26}N_4$ $[M + Na]^+$ 321.2055, found 321.2048.

biot-et-dpea. A solution of biotin-pentafluorophenol ester (1.24 g, 3.03 mmol), **4a** (0.860 g, 3.18 mmol), and triethylamine (1.11 mL, 7.95 mmol) in 40 mL DMF was allowed to stir overnight at room temperature. The DMF was removed under vacuum and the sticky tan residue was washed with diethylether until a free-flowing white solid formed. The white solid was filtered, washed with diethylether, and dried under vacuum to yield white solid (1.05 g, 70%). The solid was stored in a desiccator. ^{1}H NMR (600 MHz, DMSO-d_6) δ 8.45 (d, J = 3.6 Hz, 2H), 7.65 (t, J = 7.2 Hz, 2H), 7.51 (t, J = 4.8 Hz, 1H), 7.18 (t, J = 7.8 Hz, 4H), 6.42 (s, 1H), 6.35 (s, 1H), 4.29 (t, J = 6.0 Hz, 1H), 4.11 (t, J = 5.4 Hz, 1H), 3.07 (m, 3H), 2.56 (m, 3H), 2.20 (t, J = 7.8 Hz, 2H), 1.60 (m, 1H), 1.47 (m, 4H), 1.29 (m, 2H); ^{13}C NMR (125 MHz, DMSO-d_6) δ 171.8, 162.7, 160.3, 148.9, 136.3, 123.2, 121.2, 61.0, 59.2, 55.4, 53.7, 52.4, 36.8, 35.3, 28.3, 28.1, 25.3; HRMS (ES, MeOH) *m / z* calcd for $C_{26}H_{36}N_6O_2S$ $[M + Na]^+$ 519.2518, found 519.2504. ATR-IR (cm^{-1}, selected bands): 3223, 3072, 2928, 2856, 2817, 2359, 1698, 1641, 1591, 1567, 1548, 1473, 1433, 1324, 1264, 1148, 1121, 1051, 993, 861, 749, 596.

biot-pr-dpea was prepared analogously to the above procedure for biot-et-dpea and isolated as a tan solid (1.25 g, 86%) that was stored in a desiccator. ^{1}H NMR (600 MHz, DMSO-d_6) δ 8.46 (d, J = 4.8 Hz, 2H), 7.71 (t, J = 5.4 Hz, 2H), 7.66 (td, J = 7.8, 1.8 Hz, 2H), 7.22 (d, J = 7.8 Hz, 2H), 7.18 (t, J = 5.4 Hz, 2H), 6.41 (s, 1H), 6.35 (s, 1H), 4.29 (t, J = 6.0 Hz, 1H), 4.11 (t, J = 6.0 Hz, 1H), 3.08 (quin, J = 3.0 Hz, 1H), 2.98 (q, J = 6.0 Hz, 2H), 2.84 (s, 8H), 2.80 (m, 1H), 2.57 (d, J = 12.6 Hz, 1H), 2.04 (t, J = 7.8 Hz, 2H), 1.60 (m, 1H), 1.47 (m, 4H), 1.31 (m, 7H); ^{13}C NMR (125 MHz, DMSO-d_6) δ 171.8, 162.7, 160.3, 148.9, 136.3, 123.2, 121.2, 61.0, 59.2, 55.4, 53.4, 50.6, 36.6, 35.3, 34.9, 28.3, 28.1, 26.7, 25.4; HRMS (ES, MeOH) *m / z* calcd for $C_{27}H_{38}N_6O_2S$ $[M + Na]^+$ 533.2675, found 533.2673.

biot-bu-dpea was prepared analogously to the above procedure for biot-et-dpea and the tan solid (1.12 g, 70%) was stored in a desiccator. ^{1}H NMR (600 MHz, DMSO-d_6) δ 8.46 (d, J = 4.7 Hz, 2H), 7.71 (br t, 2H), 7.66 (t, J = 7.7 Hz, 2H), 7.22 (d, J = 7.7 Hz, 2H), 7.18 (t, J = 5.1 Hz, 2H), 6.41 (s, 1H), 6.34 (s, 1H), 4.29 (t, J = 6.2 Hz, 1H), 4.11 (t, J = 3.9 Hz, 1H), 3.08 (q, J = 6.4 Hz, 1H), 2.98 (q, J = 5.9 Hz, 2H), 2.83 (br s, 8H), 2.80 (m, 1H), 2.57 (d, J = 12.5 Hz, 1H), 2.04 (t, J = 7.4 Hz, 2H), 1.60 (m, 1H), 1.47 (m, 4H), 1.32 (m, 6H); ^{13}C NMR (125 MHz, DMSO-d_6) δ 171.8, 162.7, 160.2, 148.9, 136.3, 123.2, 121.1, 61.0, 59.2, 55.5, 53.3, 52.7, 38.2, 35.3, 34.9, 28.3, 28.1, 27.0, 25.4; HRMS (ES, MeOH) *m / z* calcd for $C_{28}H_{40}N_6O_2S$ $[M + Na]^+$ 547.2831, found 547.2824.

Preparation of Metal Complexes

[Cu^{II}(biot-et-dpea)Cl_2] H_2O was prepared by addition of solid $CuCl_2$ (0.026 g, 0.193 mmol) to a solution of biot-et-dpea (0.094 g, 0.189 mmol) in 10 mL acetonitrile. The green solution was allowed to stir for 4 h before concentrating the solution to ~ 1 mL and precipitating the complex with diethylether. The green solid was collected via filtration, which was then washed with diethyl ether, and dried under vacuum (0.097 g, 82%). ATR-IR (solid,cm^{-1}, selected bands): 3256, 3076, 2927, 1694, 1651, 1540, 1435, 1362, 1328, 1260, 1150, 1112, 1062, 1024, 761; HR-MS (ES, MeOH) *m / z* calcd for $C_{26}H_{36}Cl_2CuN_6O_2S$ $[M-Cl]^+$ 594.1611, found 594.1615. Elem. Anal. Calcd for ($C_{27}H_{40}Cl_2CuN_6O_3S$): C: 48.9; H, 6.08; N, 12.67. Found: C, 48.85; H, 6.06: N, 12.36.

[Cu^{II}(biot-pr-dpea)Cl_2] H_2O was prepared following the same procedure as for Cu^{II}(biot-et-dpea)Cl_2] H_2O and isolated as a green solid in 69% yield (0.085 g). ATR-IR (solid, cm^{-1}, selected bands): 3257, 3076, 2927, 1695, 1651, 1543, 1435, 1362, 1330, 1260, 1150, 1114, 1062, 1024, 760; HR-MS (ES, MeOH) *m / z* calcd for $C_{27}H_{38}Cl_2CuN_6O_2S$ $[M-Cl]^+$ 608.1761, found 607.1746. Elem. Anal. Calcd for ($C_{27}H_{40}Cl_2CuN_6O_3S$): C, 48.90; H, 6.08; N, 12.67. Found: C, 48.78; H, 6.04; N, 12.49.

[Cu^{II}(biot-bu-dpea)Cl_2] H_2O was prepared following the same procedure as for Cu^{II}(biot-et-dpea)Cl_2] H_2O and isolated as a green solid in 81% yield (0.090 g). ATR-IR (solid, cm^{-1}, selected bands): 3252, 3075, 2927, 1696, 1651, 1540, 1435, 1360, 1330, 1260, 1153, 1112, 1062, 1024, 760; HR-MS (ES, MeOH) *m / z* calcd for $C_{28}H_{40}Cl_2CuN_6O_2S$ $[M]^+$ 622.1918, found 622.1918. Elem. Anal. Calcd for ($C_{28}H_{42}Cl_2CuN_6O_3S$): C, 49.66; H, 6.25; N, 12.41. Found: C, 49.49; H, 6.49: N, 12.01.

Physical Methods

Instrumentation. Fourier Transform infrared spectra were collected on a Varian 800 Scimitar Series FTIR spectrometer. ^1H, ^{13}C, and ^{19}F NMR spectra were recorded at 500/600, 125, and 500 MHz, respectively. ^1H NMR spectra were reported in ppm on the δ scale and referenced to tetramethylsilane or solvent residual. The data are presented as follows: chemical shift, multiplicity (s = singlet, d = doublet, t = triplet, q = quartet, quin = quintet, m = multiplet, br = broad), coupling constant(s) in Hertz (Hz), and integration. ^{13}C NMR spectra were reported in ppm relative to $CDCl_3$ (77.23 ppm) or DMSO-d_6 (39.52 ppm). Mass spectra were measured on a MicroMass AutoSpec E, a MicroMass Analytical 7070E, or a MicroMass LCT Electrospray instrument. Electronic absorbance spectra were recorded with a Cary 50 or 8453 Agilent UV-vis spectrophotometer. X-band (9.64 GHz) and S-band (3.50 GHz) EPR spectra were recorded on a Bruker spectrometer equipped with Oxford liquid helium cryostats. The quantification of all signals is relative to a CuEDTA spin standard. The concentration of the standard was derived from an atomic absorption standard (Aldrich). For all instruments, the microwave frequency was calibrated with a frequency counter and the magnetic field with a NMR gaussmeter. A modulation frequency of 100 kHz was used for all EPR spectra. The EPR simulation software (*SpinCount*) was written by one of the authors.[5] Cyclic voltammetry was performed on a Pine WaveDriver 10 potentiostat and the data was analyzed using AfterMath.

Electronic Absorption Studies. A solution of 150 μM Sav was prepared in 50 mM MES buffer, pH 6 and transferred to a low-volume 1 cm cuvette. 18 μL of a 10 mM solution of [Cu^{II}(biot-R-dpea(OH_2)Cl]Cl in DMF was added and allowed to equilibrate for 5 minutes.

HABA Titrations. A 15 μM solution of Sav was prepared in 200 mM phosphate buffer (PB) at pH 7 and transferred to a 1 cm cuvette. 248 μL (150 equivalents) of a 20 mM solution of HABA in PB was added to ensure saturation of Sav. A solution of [Cu^{II}(biot-R-dpea(OH_2)Cl]Cl in DMF was added in 2-8 μL portions until 5 equivalents had been added. The titration was monitored by UV-Visible spectroscopy at λ_{max} = 506 nm.

EPR Experiments. To 250 μL of a 250 μM solution of Sav in 50 mM MES buffer, pH 6.0 was added 25 μL of a 10 mM solution of [Cu^{II}(biot-R-dpea(OH_2)Cl]Cl in DMF. The solution was allowed to equilibrate for 5 minutes before being transferred to an EPR tube and flash-frozen in liquid nitrogen.

All EPR spectra of the Cu ArMs with $S_{112}C$ contained varying amounts (20 to 50%) of species with features that were the same as those found in **1a**-**c** (presumably from sites in which the thiolate did not coordinate to the Cu). The spectra shown in Figure 4 are difference spectra that were obtained by appropriate subtraction of the **1a**-**c** spectra. After this subtraction, the spectra for **2a**-**2c** showed two species, but one species was a minority (10-30%) and was only obvious in the spectra of **2c** at g=1.99. The broad lineshape of the S-band spectra versus simulations can be attributed to a weak Cu-Cu spin interaction in the dimeric protein sites.

Spin Hamiltonian calculations indicate that the 12 Å Cu-Cu distance of **2a** could contribute an unresolved 3 mT splitting to the signals because of the dipolar interaction, which is comparable to the width of the signals shown in Figure 4A. The deconvolution of this broadening effect from other sources of broadening and the effect of the Cu-Cu vector orientation requires simulations that treat the nuclear spin with near degenerate perturbation theory, which is not yet available.

Electrochemical Measurements. The reduction potential of each artificial metalloprotein was determined by cyclic voltammetry using a Pine WaveDriver 10 potentiostat equipped with a Faraday cage. A solution containing 300 µL of 500 µM Sav in 100 mM MES buffer, pH6 and 60 µL of 10 mM [Cu^{II}(biot-R-dpea(OH_2)Cl]Cl in DMF was allowed to equilibrate for 5 minutes before data collection. Each metalloprotein was sampled between 2.5 and 50 mV/s. The reduction potentials were measured against a Ag/AgCl reference electrode using glassy carbon working and counter electrodes and converted to NHE.

Crystallization of [Cu^{II}(biot-et-dpea)(OH_2)$_2$]$^{2+}$⊂WT Sav. Apo-Sav protein crystals were obtained at 20°C within two days by hanging-drop vapor diffusion technique mixing 2.5 µL crystallization buffer (2.6 M ammonium sulfate, 0.1 M sodium acetate, pH 4.0) and 7.5 µL protein solution (26 mg/mL lyophilized protein in water). The droplet was equilibrated against a reservoir solution of 500 µL crystallization buffer. Subsequently, single crystals of Sav were soaked for 1 day at 20 °C in a soaking buffer, which was prepared by mixing 1 µL of a 10 mM stock solution of complex [Cu^{II}(biot-et-dpea(OH_2)Cl]Cl (in water with 100 mM $CuCl_2$), 9 µL crystallization buffer, and 0.5 µL of the original protein solution. After the soaking, crystals were transferred for 30 seconds into a cryo-protectant solution consisting of 30 % (v/v) glycerol in crystallization buffer. Next, crystals were shock-frozen in liquid nitrogen.

Crystallization of [Cu^{II}(biot-R-dpea)(S_{Cys})]$^{+}$⊂S112C Sav. Apo-Sav protein crystals were obtained at 20°C within two days by sitting-drop vapor diffusion technique mixing 1.5 µL crystallization buffer plus TCEP (2.0 M ammonium sulfate, 0.1 M sodium acetate, pH 4.0, 2 mM TCEP) and 3.5 µL protein solution (26 mg/mL lyophilized protein in water). The droplet was equilibrated against a reservoir solution of 100 µL crystallization buffer. Subsequently, single crystals of SAV were soaked for 1 day at 20 °C in a soaking buffer, which was prepared by mixing 1 µL of a 10 mM stock solution of [Cu^{II}(biot-R-dpea(OH_2)Cl]Cl in water, 9 µL crystallization buffer, and 0.5 µL of the original protein

solution. After soaking, crystals were transferred for 30 seconds into a cryo-protectant solution consisting of 30 % (v/v) glycerol in crystallization buffer. Next, crystals were shock-frozen in liquid nitrogen.

Data Processing. X-ray diffraction data were collected at the Swiss Light Source beam line X06DA and Advanced Light Source (BL8.2.1) at a wavelength of 1 Å and processed with software XDS[6] (**1a**) or iMOSFLM[7] (**2a-c**) and scaled with AIMLESS (CCP4 Suite) [7]. The structure was solved by molecular replacement using program PHASER (CCP4 Suite)[7] and the structure 2QCB from the PDB as input model with ligand and water molecules removed. For structure refinement REFMAC5 (CCP4 Suite)[8] and PHENIX.REFINE[9] were used. Ligand manipulation was carried out with program REEL using the small molecule crystal structures KAHGAB[10] (for **1a**) and CIFKOR[11] (for **2a-c**) from the Cambridge Structural Database as input models. For water picking, electron density, and structure visualization, the software COOT[12] was used. Figures were drawn with PyMOL (the PyMOL Molecular Graphics System, Version 1.5.0.5, Schrödinger, LLC). Crystallographic details, processing and refinement statistics are given in Supplementary Table S3 and S4.

Structural Results.

Crystal Color. All crystals of Sav soaked with complexes [Cu^{II}(biot-R-dpea(OH_2)Cl]Cl changed from colorless to pale blue (**1a**), violet (**2a**), or dark blue (**2b-c**).

Structural Refinement.

Overall Structures. Apo-crystals of proteins WT Sav and S112C Sav soaked with Cu-complexes [Cu^{II}(biot-R-dpea(OH_2)Cl]Cl constituted space group $I4_122$ with virtually identical unit cell parameters (Table S3). A single Sav monomer was obtained per asymmetric unit after molecular replacement. Protein residues 2-11 and 135-159 of the N- and C-terminus, respectively, were not resolved in the electron density, presumably due to disorder. Starting from the Sav monomer the biological homotetramer is generated by

application of crystallographic C2-symmetry axes along the x-, y- and z-axes of the unit cell. The overall protein structures are virtually identical to structure biotin⊂WT Sav (PDB 1STP, see Table S3).

General Complex Modeling. For all structures of apo-protein crystals soaked with the corresponding Cu-complexes the following general observations were made: i) residual electron density in the Fo-Fc map was observed in the biotin binding pocket, ii) in the biotin vestibule which is flanked by protein residues of loop-3,4^{A} (the superscript number indicates Sav monomer within tetramer) loop-4,5^{C}, loop-5,6^{A} loop-7,8^{A} and loop-7,8^{B}, and iii) an anomalous dispersion density map indicated a significant peak in the biotin vestibule superimposed with the electron density peak (Figures S4A-D and S8A-D). The residual electron density was fit with the corresponding Cu-complexes which projected Cu to the position of the strong anomalous density peak.

Structure Refinement of 1a. The complex $[Cu^{II}(\text{biot-et-dpea}(OH_2)_2]^{2+}$ was modeled with 100 % occupancy. The coordinating nitrogen atoms of the dpea ligand together with the Cu center were modeled within one plane (Figure S4A, Table S2). Additional electron density above and below this plane was observed that suggested modeling of two coordinating water molecules, resulting in a trigonal bipyramidal complex geometry around the Cu center. One of the two pyridine rings (containing N3, N3 hereafter) of dpea is nestled within loop-7,8^{A} residues S112^{A}, T114^{A}, K121^{A} , L124^{A} and two water molecules (w12 and w52) that form an H-bonding network. The second pyridine of dpea (containing N2, N2 hereafter) is in close proximity to loop-3,4^{A} and loop-7,8^{B} residues side chains N49^{A} and K121^{B}, and a glycerol molecule. One of the coordinated water molecules O3 is located close to carbonyl A83^{C} within loop-5,3^{C}. The Cu⋯Cu distance between two symmetry-related complexes is 11.3 Å (Figure S4A and S8A).

Structure Refinement of 2a. The $[Cu^{II}(\text{biot-et-dpea}(S_{Cys})]^{+}$ complex was modeled with 100 % occupancy. Side chain S112C in S112C Sav is isosteric to the serine side chain and adopts

the same rotamer as in the corresponding WT Sav structure. However, in stark contrast to WT Sav, the dpea moiety of the complex is rotated in the linker position by about 120° around the C12–N3 bond (Figure S4B, Table 2). This projects both pyridines N2 and N3 to loop-7,8^{A} and loop-7,8^{B}. N2 is tilted out of the plane and a bond is formed between Cu and S112C-Sγ (2.2 Å) to yield a pseudo-tetrahedral geometry at the Cu center (Figure S8B). The Cu···Cu distance between two Sav monomers is identical to the other structures. A relatively high residual R_{free} value and a significantly elevated overall B-factor of this structure suggest increased flexibility (Table S4).

Structure Refinement of 2b. The $[Cu^{II}$(biot-pr-dpea(S_{Cys})$]^{+}$ complex was modeled with 100 % occupancy. The Cu(DPEA) conformation is very similar to that of **2a** (Figure S4C, Table 2). However, the longer propyl linker projects the Cu(DPEA) moiety away from the biotin anchor and decreases the Cu–Sγ_{112C} distance to 2.11Å (Figure S4C). The N2–Cu–N3 angle is sharper compared to the corresponding structure of **2a** (96° vs. 127°, respectively) (Figure S8C). High flexibility of the DPEA moiety is reflected by increased atomic B-factors (Table S4).

Structure Refinement of 2c. The $[Cu^{II}$(biot-bu-dpea(S_{Cys})$]^{+}$ complex was modeled with 80 % occupancy. The Cu(DPEA) conformation is very similar to those of **2a-b** (Figure S4D, Table 2). The longer butyl linker places the Cu center further from the biotin anchor, although the Cu–Sγ_{112C} distance is similar to **2b** (2.09 Å). Additionally, the longer spacer causes movement of the S112C residue leading to a sharper $C_{\beta(S112C)}$–$S_{\gamma(S112C)}$–Cu angle of 103° versus 110° for **2a-b** (Figure S8D). High flexibility of the dpea moiety is reflected by increased atomic B-factors and decreased occupancy is attributed to steric clashing between the Cu complexes in adjacent Sav subunits (Table S4).

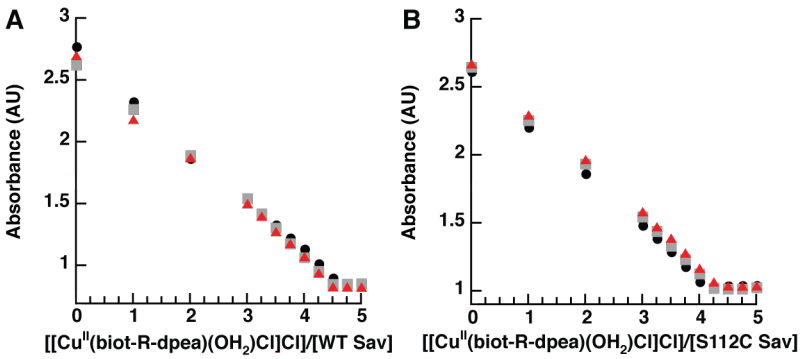

Figure S1. HABA titrations of **1a-c** (A) and **2a-c** (B). Black circle (**1-2a**), grey square (**1-2b**), red triangle (**1-2c**).

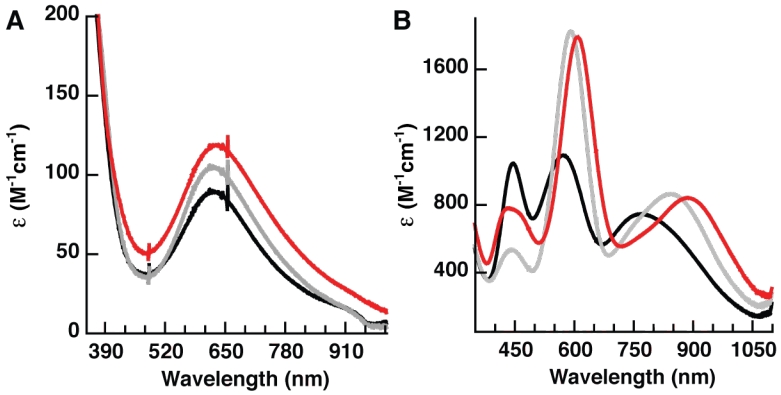

Figure S2. Electronic absorption spectra of **1a-c** (A) and **2a-c** (B). **1-2a** (black), **1-2b** (grey), and **1-2c** (red).

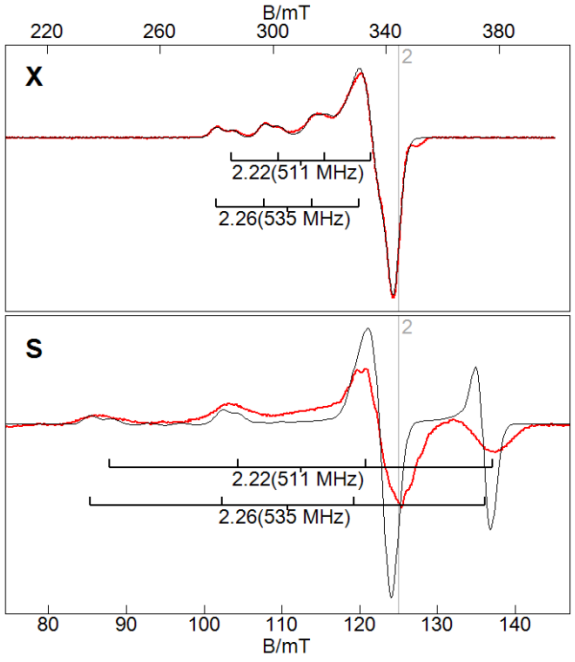

Figure S3. X- and S- band EPR spectra of **1a**. Simulations are grey lines.

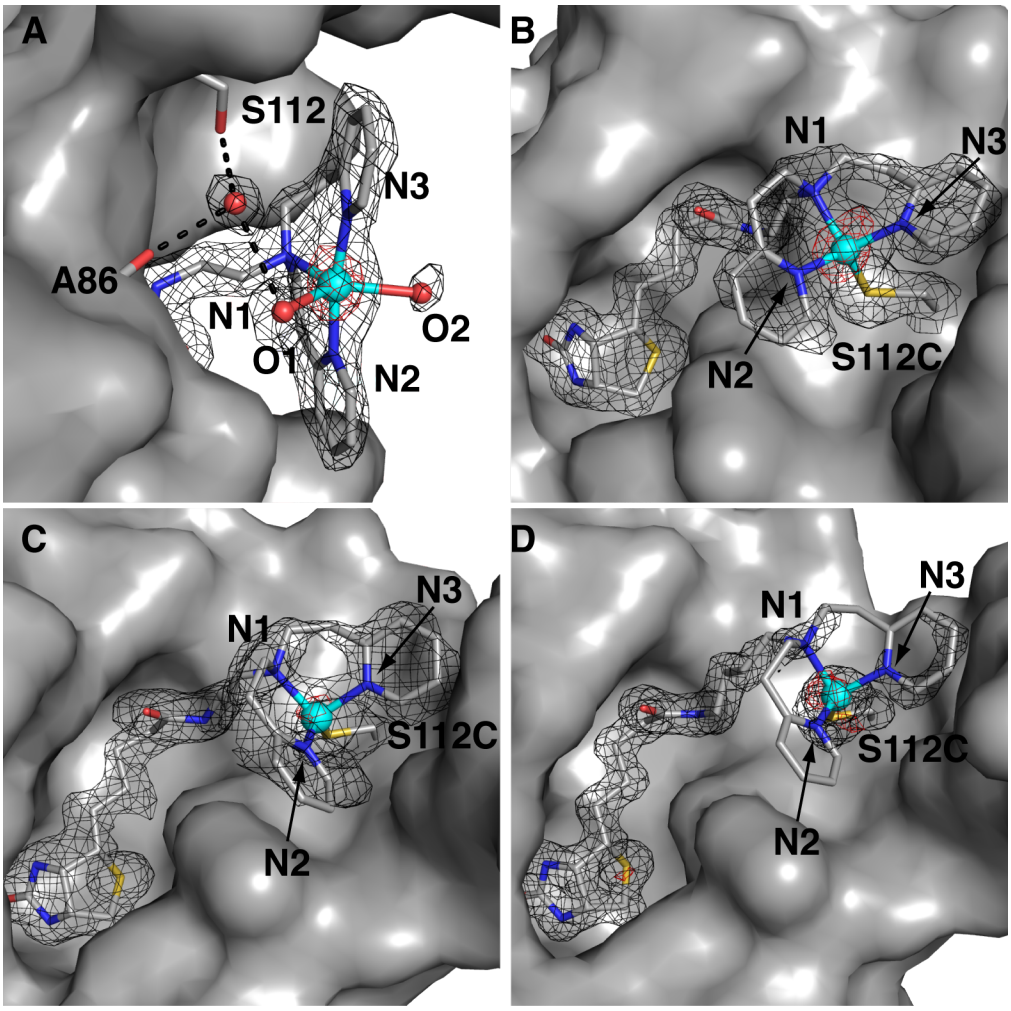

Figure S4. Close-up views of the Cu-sites in crystal structures of complexes **1a** (**A**), **2a** (**B**), **2b** (**C**), and **2c** (**D**). For clarity only one Sav monomer is displayed. The protein is displayed in surface representation and the Cu complex as well as residues 112 and 86 as sticks. The position of the ligand molecules are indicated by the $2F_o$-F_c electron density (grey, contoured at 1σ) and anomalous difference density (red, contoured at 4σ). Copper is colored in cyan and water molecules are colored in red spheres. Hydrogen bonding interactions are displayed as dashed black lines.

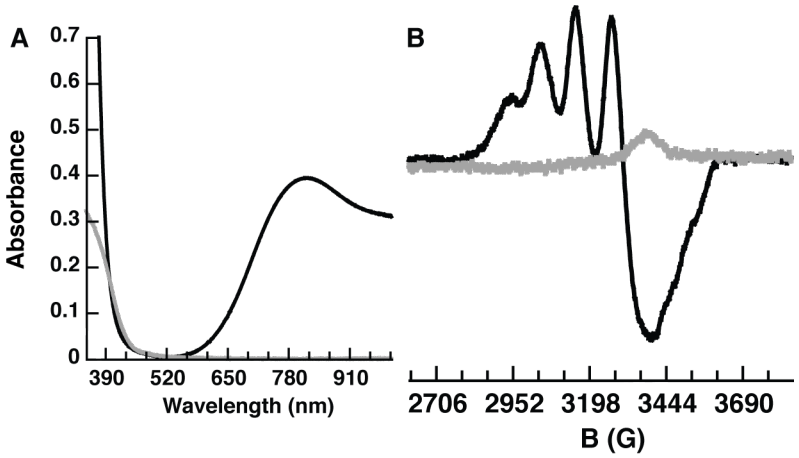

Figure S5. Absorption spectra (A) and EPR spectra (B) of [Cu^{II}(biot-pr-dpea)(Cl_2)] H_2O in DMF (black) and after reaction with one equivalent of N-(tert-Butoxycarbonyl)-L-cysteine methyl ester (grey).

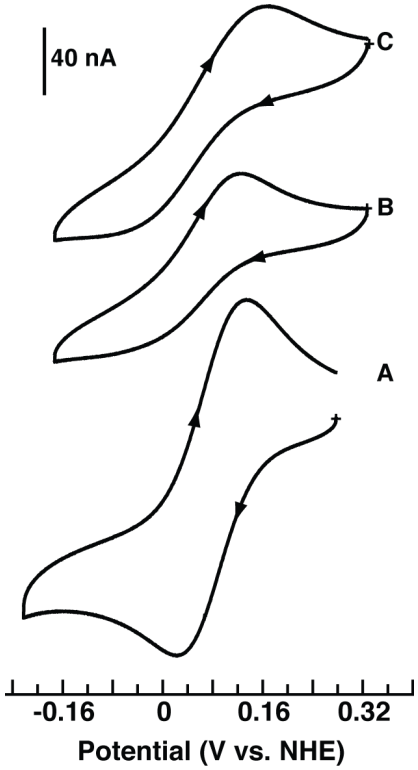

Figure S6. Cyclic voltammograms of **1a** (A), **1b** (B), and **1c** (C) collected at 10 mV/s in 100 mM MES pH 6.

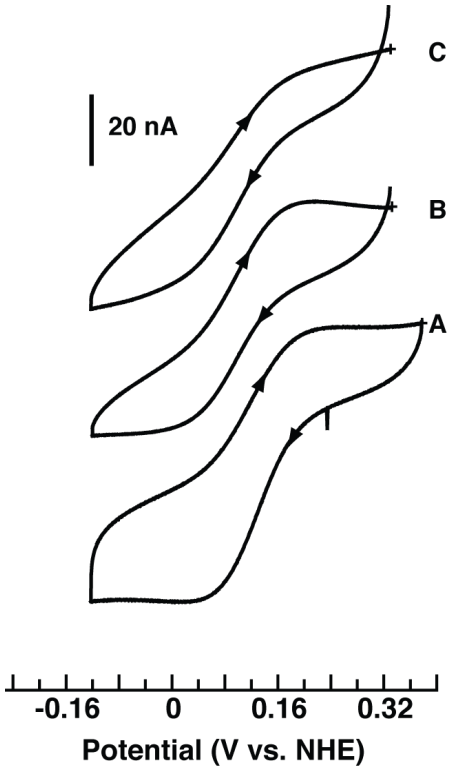

Figure S7. Cyclic voltammograms of **2a** (A), **2b** (B), and **2c** (C) collected at 5 mV/s in 100 mM MES pH 6.

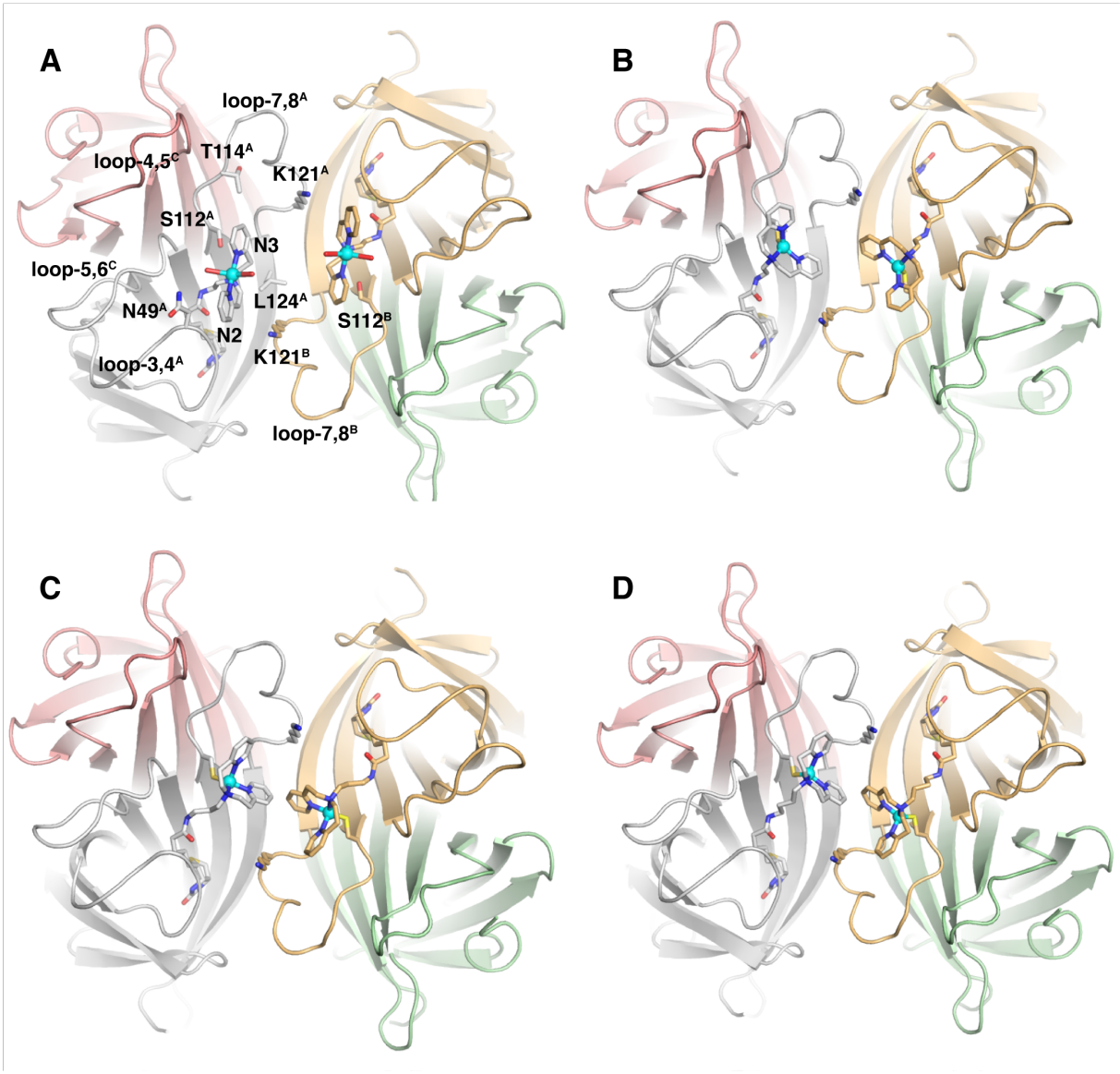

Figure S8. Views of the structures of **1a** (A), **2a** (B), **2b** (C), and **2c** (D). The Sav tetramers are represented as a cartoon and the cofactors are represented as ball and stick. Subunit A is in grey, subunit B is in tan, subunit C is pink, and subunit D is in green.

Table S1. Spectroscopic and electrochemical properties for **1a-c**.

Host	WT		
n	et (**1a**)	pr (**1b**)	bu (**1c**)
λ_{max},nm (ε_M)	625 (90)	625 (100)	626 (120)
g	2.22 2.26	2.22 2.26	2.22 2.26
A, MHz	511 535	511 535	511 535
$E_{1/2}$ mV	140	124[a]	167[a]

[a]E_a (anodic potential)

Table S2. Selected Bond Lengths (Å) and Angles (˚) for **1a**.

Host	WT
n	et (**1a**)
Cu–N1	2.08(3)
Cu–N2	2.02(3)
Cu–N3	2.09(3)
Cu–O1	2.52(3)
Cu–O2	2.46(3)
N1-Cu-N2	102(3)
N1-Cu-N3	88(3)
N2-Cu-N3	170(3)
N1-Cu-O1	104(3)
N1-Cu-O2	127(3)
N2-Cu-O1	86(3)
N2-Cu-O2	84(3)
N3-Cu-O1	94(3)
N3-Cu-O2	88(3)

Table S3. X-ray crystallography data processing and refinement statistics.

Sav Mutant	Wild type	S112C	S112C	S112C
Cu complex	$[Cu^{II}(biot\text{-}et\text{-}dpea)(OH_2)_2]^{2+}$ (**1a**)	$[Cu^{II}(biot\text{-}et\text{-}dpea)(S_{Cys})]^{2+}$ (**2a**)	$[Cu^{II}(biot\text{-}pr\text{-}dpea)(S_{Cys})]^{2+}$ (**2b**)	$[Cu^{II}(biot\text{-}bu\text{-}dpea)(S_{Cys})]^{2+}$ (**2c**)
PDB code	5K49	5L3Y	5K67	5K68
Cu complex PDB 3-letter code	SM6	SM6	SI4	SI9
Data Processing				
Unit Cell	a, b, c = 57.6 Å, 57.6 Å, 183.7 Å; α, β, γ = 90°	a, b, c = 57.8 Å, 57.8 Å, 183.3 Å; α, β, γ = 90°	a, b, c = 57.7 Å, 57.7 Å, 183.6 Å; α, β, γ = 90°	a, b, c = 57.7 Å, 57.7 Å, 183.6 Å; α, β, γ = 90°
Space group	$I4_122$	$I4_122$	$I4_122$	$I4_122$
Resolution (Å)	54.9 – 1.72	55.1 – 1.70	45.9 – 1.70	45.9 – 1.40
Highest resolution shell (Å)	1.75 - 1.72	1.73 – 1.70	1.73 – 1.70	1.42 – 1.40
R_{merge} (%)	10.8 (88.5)	11.1 (178.0)	9.2 (199.7)	6.9 (144.6)
No. of unique reflections	16931 (873)	17574 (885)	11863 (571)	31080 (1486)
Multiplicity	7.9 (7.6)	6.1 (6.5)	5.1 (4.3)	6.8 (6.6)
I/sig(I)	12.0 (1.9)	7.6 (0.9)	9.7 (0.7)	12.7 (1.0)
Completeness	99.7 (98.9)	99.8 (100)	66.9 (64.3)	99.8 (98.8)
CC(1/2)	1.00 (0.68)	1.00 (0.57)	1.00 (0.34)	1.00 (0.40)
Structure Refinement				
R_{work}	0.13	0.18	0.20	0.14
R_{free}	0.17	0.24	0.23	0.18
Rmsd bond length (Å)	0.0294	0.032	0.0192	0.0317
Rmsd bond angle (°)	2.5839	2.7865	2.1818	3.915
Rmsd compared to biotin-SAV WT (PDB 1STP) (Å)	0.78	0.71	0.70	0.76
No ligands				
Cu complex	1	1	1	1
Water	67	45	32	68
Glycerol	1	-	1	-
acetate	1	-	-	-

Table S4. Summary of structural details.

PDB code	5K49	5L3Y	5K67	5K68
Complex	**1a**	**2a**	**2b**	**2c**
Electron density at Cu in FoFc omit map (σ)	15	21	12	16
Anomalous dispersion density at Cu (σ)	12	11	5	7
Geometry of Cu complex	Trigonal bipyramidal	distorted tetrahedral	Trigonal monopyramidal	Trigonal monopyramidal
Coordination number of Cu complex	5	4	4	4
Conformation of Cu complex	parallel to loop 7,8	orthogonal to loop 7,8	orthogonal to loop 7,8	orthogonal to loop 7,8
Occupancy of Cu complex (%)	100	100	100	80
B-factor (Å^2) Overall protein S112X Loop-7,8 Cu complex DPEA Cu	 20 15 20 30 45 41	 26 22 25 35 51 40	 23 21 23 40 71 59	 20 16 19 39 63 44
Distance Cu-Cu (Å)	11	12	10	10

References.

(1) Pangborn, A. B.; Giardello, M. A.; Grubbs, R. H.; Rosen, R. K.; Timmers, F. J. *Organometallics* **1996**, *15*, 1518.
(2) Chambers, J. M.; Lindqvist, L. M.; Webb, A.; Huang, D. C. S.; Savage, G. P.; Rizzacasa, M. A. *Org. Lett.* **2013**, *15*, 1406.
(3) Leaver, S. A.; Palaniandavar, M.; Kilner, C. A.; Halcrow, M. A. *Dalton Trans.* **2003**, 22, 4224.
(4) Incarvito, C.; Lam, M.; Rhatigan, B.; Rheingold, A. L.; Qin, C. J.; Gavrilova, A. L.; Bosnich, B. **2001**,23, 3478.
(5) Petasis, D. T.; Hendrich, M. P. *Methods Enzymol.* **2015**, *563*, 171-208.
(6) Kabsch, W. *Acta. Crystallogr. D Biol. Crystallogr.* **2010**, *66*, 125.
(7) Evans, P. R. *Acta. Crystallogr. D Biol. Crystallogr.* **2011,** *D67*, 282.
(8) Murshudov, G. N.; Vagin, A. A.; Dodson, E. J. *Acta. Crystallogr. D Biol. Crystallogr.* **1997**, *53*, 240.
(9) Adams, P. D.; Afonine, P. V.; Bunkóczi, G.; Chen, V. B.; Davis, I. W.; Echols, N.;

Headd, J. J.; Hung, L.-W.; Kapral, G. J.; Grosse-Kunstleve, R. W.; McCoy, A. J.; Moriarty, N. W.; Oeffner, R.; Read, R. J.; Richardson, D. C.; Richardson, J. S.; Terwilliger, T. C.; Zwart, P. H. *Acta. Crystallogr. D Biol. Crystallogr.* **2010**, *66*, 213.
(10) Blain, I.; Giorgi, M.; De Riggi, I.; Reglier, M. *Eur. J. Inorg. Chem.* **2000**, *2000*, 393.
(11) Karlin, K. D.; Shi, J.; Hayes, J. C.; McKown, J. W. *Inorg. Chimica. Acta.* **1984**, *91*, L3.
(12) Emsley, P.; Cowtan, K. *Acta. Crystallogr. D Biol. Crystallogr.* **2004**, *60*, 2126.